nature COMMUNICATIONS

ARTICLE

DOI: 10.1038/s41467-017-00916-7 OPEN

# Binary temporal upconversion codes of $Mn^{2+}$-activated nanoparticles for multilevel anti-counterfeiting

Xiaowang Liu[1], Yu Wang[2], Xiyan Li[1], Zhigao Yi[1], Renren Deng[1], Liangliang Liang[1], Xiaoji Xie[3], Daniel T.B. Loong[4], Shuyan Song[5], Dianyuan Fan[2], Angelo H. All[4,6,7], Hongjie Zhang[5], Ling Huang[3] & Xiaogang Liu[1,2,8]

Optical characteristics of luminescent materials, such as emission profile and lifetime, play an important role in their applications in optical data storage, document security, diagnostics, and therapeutics. Lanthanide-doped upconversion nanoparticles are particularly suitable for such applications due to their inherent optical properties, including large anti-Stokes shift, distinguishable spectroscopic fingerprint, and long luminescence lifetime. However, conventional upconversion nanoparticles have a limited capacity for information storage or complexity to prevent counterfeiting. Here, we demonstrate that integration of long-lived $Mn^{2+}$ upconversion emission and relatively short-lived lanthanide upconversion emission in a particulate platform allows the generation of binary temporal codes for efficient data encoding. Precise control of the particle's structure allows the excitation feasible both under 980 and 808 nm irradiation. We find that the as-prepared $Mn^{2+}$-doped nanoparticles are especially useful for multilevel anti-counterfeiting with high-throughput rate of authentication and without the need for complex time-gated decoding instrumentation.

[1] Department of Chemistry, National University of Singapore, Singapore 117543, Singapore. [2] SZU-NUS Collaborative Innovation Center for Optoelectronic Science & Technology, Key Laboratory of Optoelectronic Devices and Systems of Ministry of Education and Guangdong Province, College of Optoelectronic Engineering, Shenzhen University, Shenzhen 518060, China. [3] Key Laboratory of Flexible Electronics & Institute of Advanced Materials, Jiangsu National Synergetic Innovation Center for Advanced Materials, Nanjing Tech University, Nanjing 211816, China. [4] Singapore Institute of Neurotechnology (SINAPSE), National University of Singapore, Singapore 117456, Singapore. [5] State Key Laboratory of Rare Earth Resource Utilization, Changchun Institute of Applied Chemistry, Chinese Academy of Sciences, Changchun 130022, China. [6] Department of Biomedical Engineering, Johns Hopkins School of Medicine, Baltimore, MD 21205, USA. [7] Department of Neurology, Johns Hopkins School of Medicine, Baltimore, MD 21205, USA. [8] Institute of Materials Research and Engineering, Agency for Science, Technology and Research, Singapore 117602, Singapore. Correspondence and requests for materials should be addressed to L.H. (email: iamlhuang@njtech.edu.cn) or to X.L. (email: chmlx@nus.edu.sg)

The emission color of luminescent materials plays a crucial role in encoding information for anti-counterfeiting[1–3] and optical multiplexing[4, 5]. Lanthanide-doped upconversion nanoparticles are particularly suitable for such applications because they can be readily deposited or patterned as films from solution to create multicolor barcodes under a single-wavelength excitation or through thermal radiation[6–10]. For example, three primary colors can be readily obtained through the use of Er-Tm (red), Yb-Er (green), and Yb-Tm (blue) dopant pairs[11–13]. In addition, the strong dependence of the color output on the excitation source, such as power density, pulse duration and excitation wavelength, provides an added benefit in fine-tuning the emission profiles without the need for particle composition modification[14–18]. Furthermore, a low threshold of pumping (down to 1 W $cm^{-2}$) is required to realize upconversion emission, making these nanoparticles an ideal target for practical and high-capacity information storage[19–22].

Despite the attractions, the use of color elements for multiplexing to enhance data storage density and security remains a formidable challenge. An obvious bottleneck is the unavoidable overlap in the emission spectra of the nanoparticles under study. Alternatively, time-domain codes of lanthanide-doped nanoparticles have proven effective in adding flexibility in high-density data storage and another dimension of complexity to combat counterfeiting[23–25]. However, the need for time-gated instrumentation and a tedious data-decoding process poses a considerable constraint for practical use. One promising strategy that simplifies the coding and decoding procedure is the integration of long-lived emission (>15 ms) with conventional upconversion emission for distinct binary temporal scales that can be visualized on excitation at a single wavelength.

Optical nanoparticles that simultaneously display a long-lived emission and a relatively short-lived emission are generally difficult to prepare by direct coating of conventional afterglow materials such as $MAl_2O_4:Eu^{2+}/Dy^{3+}$ (M=Ca or Sr) onto lanthanide-doped nanocrystals, typically composed of NaGd(or Y)$F_4$:Yb/Er (or Tm). This difficulty is largely due to the challenge of mitigating the large lattice mismatch between the two materials. Co-doping of transition metal ions having a long-lived emission nature and lanthanide dopants within a host lattice has also proven ineffective owing to the weak energy transfer between the two optical centers[26]. In addition, optical incompatibility between the pair in some cases can even lead to deleterious cross-relaxation, resulting in rapid quenching of excitation energies[27–29].

Here, we reason that upconversion nanoparticles possessing binary color scales can be obtained by spatially controlled co-doping of manganese (II) ions into hexagonal-phased $NaLnF_4$ (Ln = lanthanide) lattices. First, the spin-forbidden transition nature of the $3d^5$ configuration of $Mn^{2+}$ permits long-lived emission up to several milliseconds, a duration which is discernible by the naked eye[30–33]. Furthermore, the low phonon energy of $NaLnF_4$ lattice is likely to decrease the probability of nonradiative transitions, thereby leading to enhanced upconversion efficiency for both emitters. By making use of energy migrators to link the two emitting centers, we report the access to binary temporal upconversion codes benefiting from the large lifetime difference in their emissions. We find that a precise control over core-shell structures not only allows for the creation of a library of short-lived color codes but also makes it possible to excite the nanoparticles under both 980 and 808 nm irradiation[34–42]. We show that these nanomaterials are particularly attractive for multilevel anti-counterfeiting by taking advantage of the parallel implementation of optical readout at high-throughput rates.

## Results

**Synthesis of basic binary temporal upconversion codes**. The particle design for achieving long-lived upconversion encoding is shown in Fig. 1a. Hexagonal-phased $NaGdF_4$:Mn and $NaGdF_4$:Yb/Tm(49/1 mol%) are used as core and first shell layer, respectively, to enable $Mn^{2+}$ emission through an energy migration upconversion process (Fig. 1b)[43–45]. Succeeding layers made of pure or doped $NaYF_4$ materials can be conveniently passivated in support of color tuning of the short-lived lanthanide emission while preserving the long-lived luminescence of $Mn^{2+}$.

To validate our hypothesis, we first prepared hexagonal-phased $NaGdF_4$:Mn core nanoparticles by a hydrothermal method. In the synthesis, we observed a hexagonal-to-cubic phase transformation at a high doping concentration of $Mn^{2+}$ (40 mol%)[27, 29], as revealed by powder X-ray diffraction studies (Supplementary Fig. 1). Inductively coupled plasma atomic emission spectroscopy analysis showed that there are big discrepancies between the designed and measured concentrations of $Mn^{2+}$ in core nanoparticles (Supplementary Fig. 2 and Supplementary Table 1), suggesting the low solubility of $Mn^{2+}$ in the hexagonal-phased $NaGdF_4$.

We next performed epitaxial growth of $NaYF_4$:Yb/Tm(49/1 mol%) and $NaYF_4$ layers onto the as-prepared $NaGdF_4$:Mn(30 mol%) cores by a combination of coprecipitation and thermal decomposition methods (Supplementary Fig. 3). After implementing the epitaxial growth, the resultant nanoparticles were confirmed to retain hexagonal phase (Supplementary Fig. 1). Transmission electron microscopy (TEM) showed that the epitaxial growth led to an obvious increase in the size of the nanoparticles from 12 to 17 nm (Fig. 2a), accompanying with a slight morphological change from short-rod-like to spherical shape. The morphological change can be ascribed to the occurrence of oleic acid-assisted etching during the high-temperature shell-growth process (290 °C)[46]. High-resolution TEM imaging revealed the single-crystalline nature of the as-prepared core-shell-shell nanoparticles with a measured *d*-spacing of 0.51 nm (Fig. 2a, inset), which is in good agreement with the lattice spacing in the (100) planes of hexagonal phase $NaGdF_4$.

Optical characterization showed a gradual increase in the emission intensity upon subsequent growth of $NaYF_4$:Yb/Tm (49/1 mol%) and $NaYF_4$ layers onto the as-prepared $NaGdF_4$:Mn (30 mol%) core nanoparticles (Supplementary Fig. 4), implying the formation of core-shell and core-shell-shell nanoparticles. The emission profile of the resulting multilayer nanoparticles (Fig. 2b) showed a broad $Mn^{2+}$ emission in the region of 490–625 nm, in addition to characteristic emission bands for $Tm^{3+}$ centered at 450, 475, 646, and 694 nm. The generation of upconversion $Mn^{2+}$ luminescence is likely a result of Gd-sublattice-mediated energy migration, made evident by the observation of a notable decrease in the lifetime of $Gd^{3+}$ (311 nm, $^6P_{7/2} \rightarrow {}^8S_{7/2}$) from 6.5 to 4 ms after the placement of $Mn^{2+}$ ions into the particle's core (Supplementary Fig. 5). It was found that the upconversion emission intensity of $Mn^{2+}$ is highly dependent on the doping level (2.5–30 mol%) of $Mn^{2+}$ in the core (Supplementary Fig. 6). On a separate note, the emission intensity of $Mn^{2+}$ ions under investigation is about ten times stronger than that obtained from cubic-phased equivalents (Supplementary Figs 7 and 8). Taken together, these results suggest that hexagonal-phased $NaGdF_4$ lattice is more suitable for achieving energy transfer and energy migration upconversion for both lanthanides and transition metal ions, as opposed to cubic-phased counterpart.

The lifetime of $Mn^{2+}$ emission was found to be much longer than that of $Tm^{3+}$ emission (Fig. 2c). As expected, we did observe a strong green luminescence after disappearance of the short-lived $Tm^{3+}$ emission. The lifetime of $Mn^{2+}$ emission from the multilayer nanoparticles was estimated to be 39 ms, which is about 65 times longer than that of $Tm^{3+}$ emission centered at 475 nm (Fig. 2d). We ascribed the long-lived $Mn^{2+}$ upconversion emission mainly to the spin-forbidden nature of its $^4T_1 \rightarrow {}^6A_1$ transition. In addition, the multilayer structure of the nanoparticle should also partially contribute to the long lifetime of the

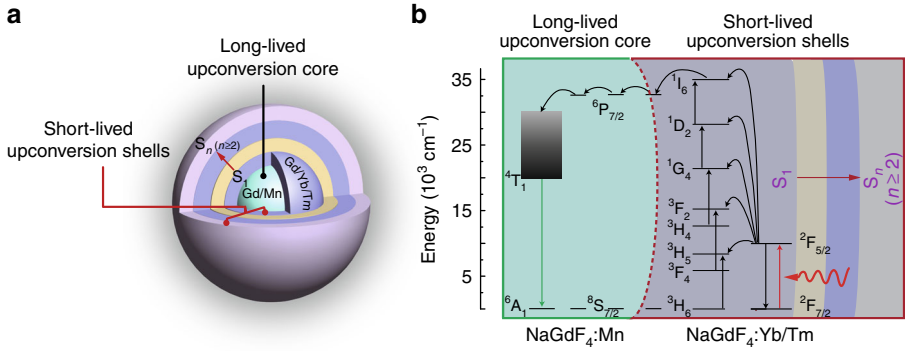


**Fig. 1** Rational design of binary temporal upconversion codes through $Mn^{2+}$ codoping. **a** Structure design of a multilayer nanoparticle for simultaneously displaying short- and long-lived upconversion emissions. Noted that $NaGdF_4$:Mn(30 mol%) and $NaGdF_4$:Yb/Tm(49/1 mol%) are exploited as core and first shell ($S_1$) of the multilayer nanoparticle to achieve long-lived $Mn^{2+}$ luminescence through Gd-sublattice-mediated energy migration. Other characteristic lanthanide emissions from the nanoparticle can be realized by further coating additional shell layers ($S_n$) with different lanthanide compositions: strategy i $S_2 = NaYF_4$, ii $S_2 = NaYF_4$:A (A = $Eu^{3+}$, $Eu^{3+}$/$Tb^{3+}$ or $Tb^{3+}$), iii $S_2 = NaYF_4$, $S_3 = NaYF_4$:Yb/Er (5/0.05, 20/2 or 50/0.05 mol%), iv $S_2 = NaYF_4$:Nd (20 mol%), $S_3 = NaYF_4$:Nd/Yb/Er(1/30/0.5 or 2/10/1 mol%), and v $S_2 = NaYF_4$, $S_3 = NaYF_4$:Nd (20 mol%), $S_4 = NaYF_4$:Nd/Yb/Er (2/10/1 mol%). **b** Proposed energy transfer pathway between the core and shell layers accounting for the simultaneous generation of short- and long-lived upconversion luminescence under excitation at 980 nm

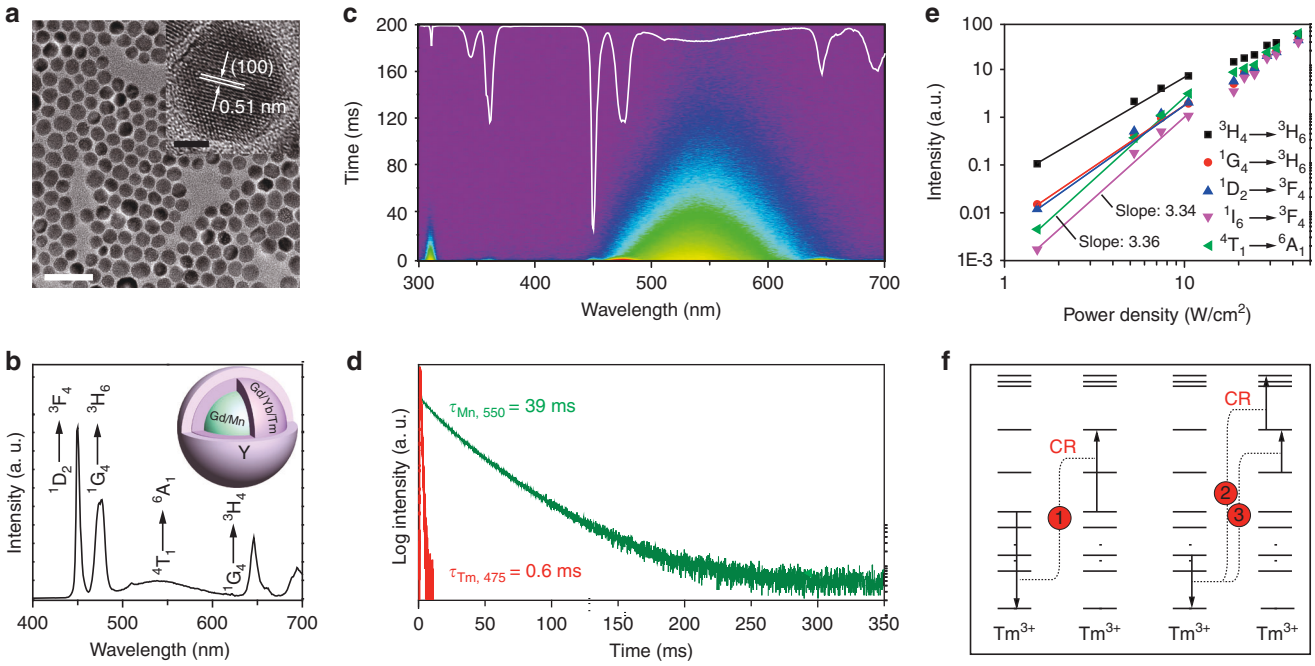


**Fig. 2** Characterization of multilayer nanoparticles of $NaGdF_4$:Mn (30 mol%)@$NaGdF_4$:Yb/Tm (49/1 mol%)@$NaYF_4$. **a** TEM image of the as-prepared upconversion nanoparticles, *scale bar*, 50 nm. (*Inset*: high-resolution TEM imaging of a single core-shell-shell nanoparticle, *scale bar*, 5 nm). **b** Emission profile of the as-prepared nanoparticles under excitation at 980 nm (power density: 30 W cm$^{-2}$). **c** Time-resolved spectrum of the as-prepared $Mn^{2+}$-doped upconversion nanoparticles. **d** Lifetime comparison of $Mn^{2+}$ emission (550 nm, $^4T_1 \rightarrow {}^6A_1$) and $Tm^{3+}$ (475 nm, $^1D_2 \rightarrow {}^3F_4$) of the as-prepared $Mn^{2+}$-doped nanoparticles recorded in aqueous solution at room temperature. **e** Power density dependence of the upconverted $Tm^{3+}$ and $Mn^{2+}$ emissions. Note that the slopes of power-dependent emission centered at 345 nm for $Tm^{3+}$ and at 550 nm for $Mn^{2+}$ are measured to be 3.34 and 3.36, respectively. **f** Proposed cross-relaxation (CR) processes between two neighboring $Tm^{3+}$ ions, accounting for the experimentally observed lower exponential power dependence of the $Tm^{3+}$ and $Mn^{2+}$ emissions

$Mn^{2+}$ upconversion emission because this design can effectively lead to the separation of $Yb^{3+}$ and $Mn^{2+}$ and thereby prevent the back-energy transfer from $Mn^{2+}$ to $Yb^{3+}$ (ref. [47]). The prevention of the $Mn^{2+}$-to-$Yb^{3+}$ back-energy transfer is likely to be crucial for retaining the intrinsically long-lifetime of $Mn^{2+}$ upconversion emission. For example, a much shorter lifetime of $Mn^{2+}$ upconversion emission (19 ms) was observed in homogeneously doped nanoparticles of $NaYF_4$:Yb/Mn(5/30 mol%) (Supplementary Fig. 9).

**Simulation studies**. To provide insight into the energy transfer within the $Mn^{2+}$-doped nanoparticles, we performed power-dependent study of the upconverted $Tm^{3+}$ and $Mn^{2+}$ emissions. We recorded a slope of 3.34 for the violet emission of $Tm^{3+}$ centered at 345 nm and a slope of 3.36 for the green emission of $Mn^{2+}$ centered at 550 nm (Fig. 2e). This result is quite surprising because we expect that a five-photon excitation should be the dominant process as outlined in Fig. 1b. To clarify this point, we further carried out energy transfer simulation, with or without

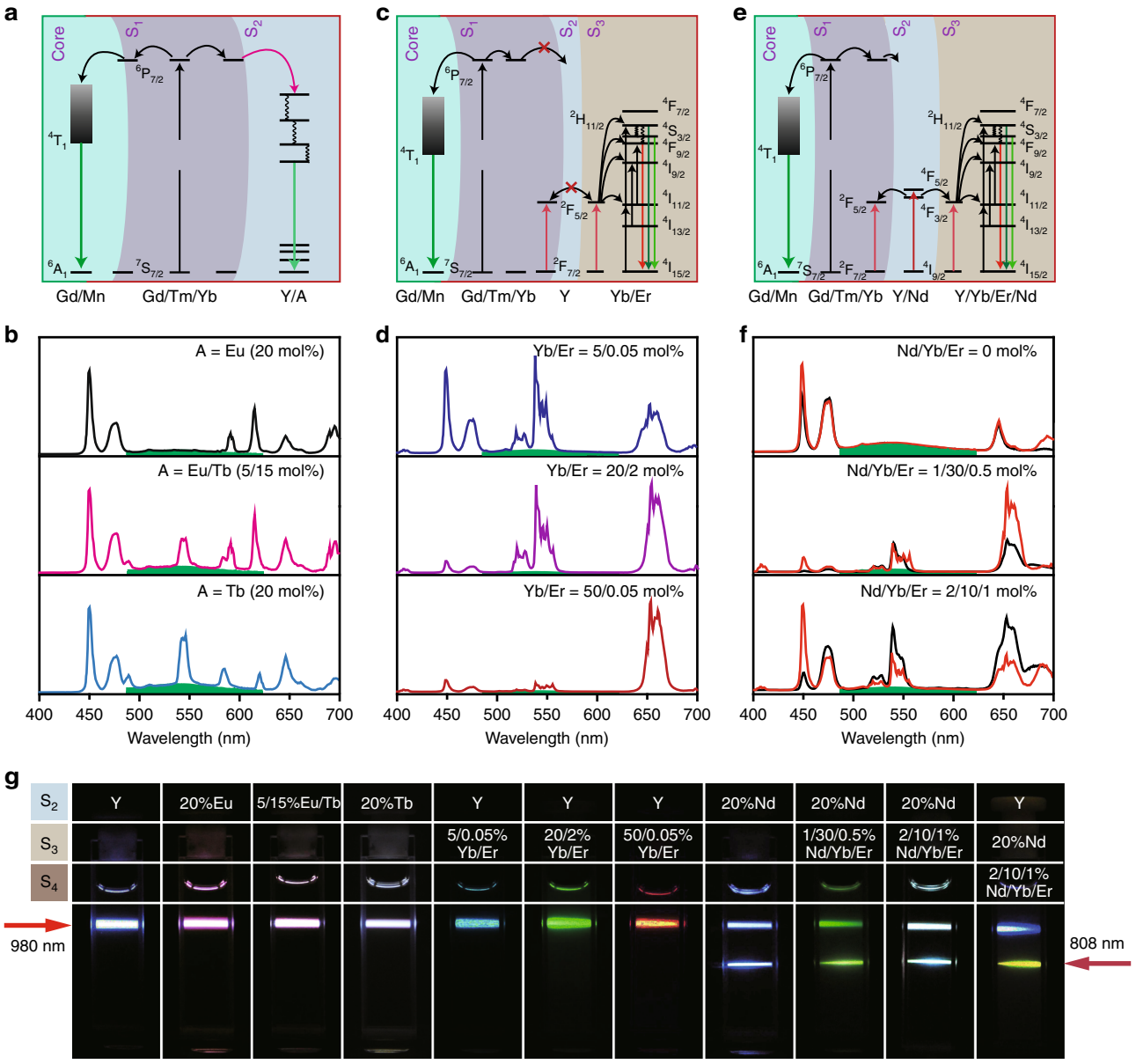


**Fig. 3** Synthetic strategies for tuning short-lived upconversion emission. **a** Doping of lanthanide activators (A = $Eu^{3+}$, $Eu^{3+}$/$Tb^{3+}$ or $Tb^{3+}$) into the outmost shell ($S_2$) of $NaYF_4$ to realize interfacial energy transfer. In contrast to energy migration strategy, interfacial energy transfer mainly occurs at the interface and has less effect on the $Mn^{2+}$ luminescence. **b** Representative emission profiles of the as-prepared $NaGdF_4$:Mn(30 mol%)@$NaGdF_4$:Yb/Tm(49/1 mol%)@$NaYF_4$:A (A = $Eu^{3+}$, $Eu^{3+}$/$Tb^{3+}$ or $Tb^{3+}$) nanoparticles. **c** Strategy involving the addition of $NaYF_4$ ($S_2$) and $NaYF_4$:Yb/Er ($S_3$) layers. Note that the emission dependence of the $NaYF_4$:Yb/Er shell on the relative doping level of Yb/Er provides an additional means to modulate the emission color of the nanoparticles. **d** Emission profiles of the as-prepared $NaGdF_4$:Mn(30 mol%)@$NaGdF_4$:Yb/Tm(49/1 mol%)@$NaYF_4$@$NaYF_4$:Yb/Er(5/0.05, 20/2 or 50/0.05) nanoparticles. **e** Doping of $Nd^{3+}$ into the $NaYF_4$ shell ($S_2$) allows the excitation to be carried out either under 980 or 808 nm. Notably, the small-sized and curved arrow between $S_1$ and $S_2$ layers is used to represent a much weaker interfacial energy transfer from $Gd^{3+}$ to $Nd^{3+}$ relative to energy migration from $Gd^{3+}$ in the $S_1$ layer to $Mn^{2+}$ in the core. **f** Emission spectra of $NaGdF_4$:Mn(30 mol%)@$NaGdF_4$:Yb/Tm(49/1 mol%)@$NaYF_4$:Nd(20 mol%) nanoparticles and the corresponding multilayer nanoparticles passivated with $NaYF_4$:Nd/Yb/Er (*x* mol%) (*x* = 1/30/0.5 or 2/10/1) under excitation at 980 (*red curve*) and 808 nm (*black curve*). The pump powers of the 980 and 808 nm lasers were fixed at 1 and 4 W for spectral measurement, respectively. **g** Luminescence photographs showing multicolour tuning of the steady upconversion of the as-prepared nanoparticles under excitation at 980 or 808 nm. The energy transfer from $Nd^{3+}$ → $Yb^{3+}$ → $Tm^{3+}$ → $Gd^{3+}$ → $Mn^{2+}$ under excitation at 808 nm can be largely suppressed by growth of an inert shell between $NaYF_4$:Nd (20 mol%) and $NaGdF_4$:Yb/Tm(49/1 mol%), and thus different color outputs can be generated upon excitation at 980 and 808 nm (Supplementary Fig. 19)

consideration of $Tm^{3+}$-$Tm^{3+}$ cross-relaxation, by employing a set of rate equations (Supplementary Figs. 10 and 11). Interestingly, the simulated results with the consideration of the $Tm^{3+}$-$Tm^{3+}$ cross-relaxation are in good agreement with our experimental results (Fig. 2f), as supported by the generation of similar slopes in the fitting curves within the low power density region. Taken together, these findings suggest that the green upconversion emission of $Mn^{2+}$ is likely to be the result of a five-photon upconversion process; and the experimentally observed lower exponential power dependence of the emission is due to the occurrence of cross-relaxation between neighboring $Tm^{3+}$ ions (Supplementary Note 1).

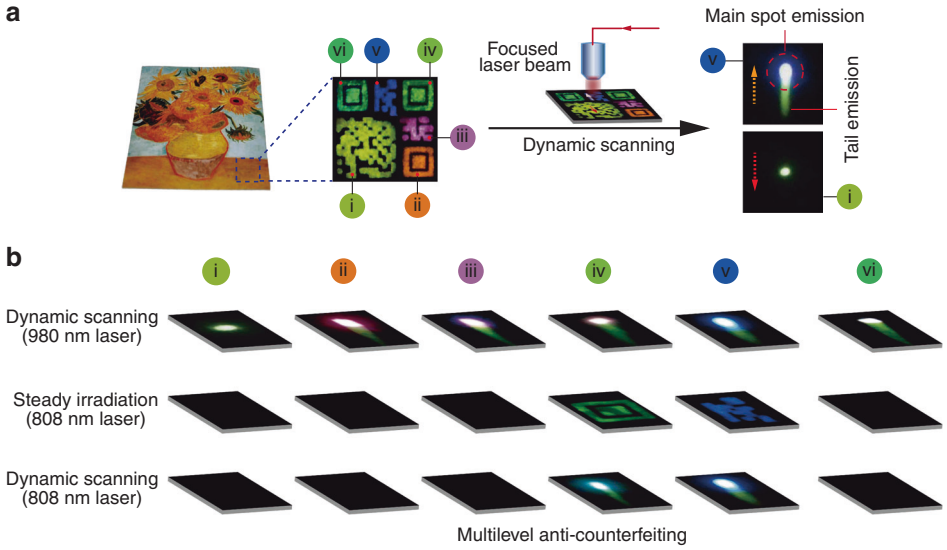


**Fig. 4** Multilevel anti-counterfeiting application with $Mn^{2+}$-activated core-shell nanoparticles. **a** General design of the 2D patterns (i to vi) made with nanoparticles of different composition. Steady irradiation with a 980 nm laser (6 W $cm^{-2}$) leads to multicolor features of the patterns, while dynamic scanning of the patterns with a focused laser beam (64 W $cm^{-2}$) gives rise to a different scenario. Unlike purely lanthanide-doped nanoparticles with only a bright spot of emission emerging from pattern i under the dynamic scanning, the as-prepared $Mn^{2+}$-doped nanoparticles show a bright spot of emission with a *green-colored tail* from pattern v. **b** Emission profiles of the patterns recorded under different irradiation conditions. Each pattern varies significantly in emission color under dynamic scanning at 980 nm. Steady irradiation or dynamic scanning at 808 nm of the patterns iv and v, made with $Nd^{3+}$-sensitized nanoparticles, can provide a similar level of readout to that on 980 excitation. Nanoparticles used for generating the patterns: i $NaYF_4$:Yb/Er (20/2 mol%); ii $NaGdF_4$:Mn (30 mol%)@$NaGdF_4$:Yb/Tm (49/1 mol%)@$NaYF_4$@$NaYF_4$:Yb/Er (50/0.05 mol%); iii $NaGdF_4$:Mn (30 mol%)@$NaGdF_4$:Yb/Tm(49/1 mol%)@$NaYF_4$:Eu(20 mol%); iv $NaGdF_4$:Mn(30 mol%)@$NaGdF_4$:Yb/Tm(49/1 mol%)@$NaYF_4$:Nd(20 mol%)@$NaYF_4$:Nd/Yb/Er(2/10/1 mol%); v $NaGdF_4$:Mn(30 mol%)@$NaGdF_4$:Yb/Tm(49/1 mol%)@$NaYF_4$:Nd(20 mol%); and vi $NaGdF_4$:Mn(30 mol%)@$NaGdF_4$:Yb/Tm(49/1 mol%)@$NaYF_4$@$NaYF_4$:Yb/Er (5/0.05 mol%)

**Enriching the variety of short-lived upconversion codes**. To add more flexibility into tuning the short-lived upconversion emission of the $Mn^{2+}$-doped nanoparticles, we set out to examine the possibility of doping lanthanide activators (denoted as A: $Eu^{3+}$, $Eu^{3+}$/$Tb^{3+}$, or $Tb^{3+}$) into the outmost shell of $NaYF_4$ (Fig. 3a and Supplementary Fig. 12). As anticipated, an interfacial energy transfer from $Gd^{3+}$ to a given lanthanide activator occurred, leading to a characteristic emission band of the activator in the visible region (Fig. 3b). Importantly, the variation in composition had a marginal influence on the optical properties of $Mn^{2+}$ ions (Supplementary Fig. 13). In contrast, an energy migration transfer process involving doping of $Tb^{3+}$ (20 mol%) into the outmost layer of $NaGdF_4$ led to a substantial decrease in the emission lifetime (Supplementary Fig. 14). The difference lies in the fact that the interfacial energy transfer mainly occurs at a few atomic layers at the interface and thus leads to less competition with $Mn^{2+}$ in trapping the excitation energy from excited $Gd^{3+}$ ions[48].

To enrich the color diversity of the short-lived upconversion emission, we further doped $Er^{3+}$ ions into the nanoparticles (Fig. 3c). An additional layer of $NaYF_4$ was used to separate the core and the shell comprising the $Er^{3+}$ ions. The emission dependence of $Er^{3+}$ on the $Yb^{3+}$ content provides a precise control over the emission profile of the resultant nanoparticles. For example, intense white, green, or red color can be readily generated by varying the ratio of $Yb^{3+}$ to $Er^{3+}$ ions (5/0.05, 20/2 or 50/0.05 mol%) that are encapsulated in the outmost shell of the nanoparticles (Fig. 3d and Supplementary Fig. 15)[49]. In these cases, the emission profiles of the long-lived $Mn^{2+}$ luminescence become indistinguishable due to the spectral overlap with the emission bands of $Er^{3+}$ at 520 and 540 nm.

Remarkably, the distinct upconversion emission of $Mn^{2+}$ in green could be clearly visualized after a short time interval when all lanthanide emissions ceased. This supports the lifetime measurements that the decay kinetics of $Mn^{2+}$ emission is almost irrespective to the epitaxially grown shell of $NaYF_4$:Yb/Er in presence of an inert shell layer of $NaYF_4$ (Supplementary Fig. 16). Control experiments showed that multilayer nanoparticles without the $NaYF_4$ layer generate merely a yellow emission from the lanthanides, but not the long-lasting luminescence from $Mn^{2+}$ (Supplementary Fig. 17). This observation is likely due to the preferential energy transfer from $Yb^{3+} \rightarrow Er^{3+}$ or caused by $Yb^{3+}$–$Yb^{3+}$ energy migration from the inner layer of $NaGdF_4$:Yb/Tm(49/1 mol%) to the outer layer of $NaYF_4$:Yb/Er.

**Generation of binary temporal codes under 808 nm excitation**. An efficient energy transfer from $Nd^{3+}$ to $Yb^{3+}$ ions allows the extension of the excitation wavelength of $Mn^{2+}$-doped nanoparticles from 980 to 808 nm[50–52]. This was validated through an epitaxial growth of $NaYF_4$:Nd(20 mol%) on $NaGdF_4$:Mn(30 mol%)@$NaGdF_4$:Yb/Tm(49/1 mol%) core-shell nanoparticles (Fig. 3e and Supplementary 18a). The excitation energy is first harvested by $Nd^{3+}$ ions followed by energy transfer to $Yb^{3+}$ and then energy relay through $Yb^{3+} \rightarrow Tm^{3+} \rightarrow Gd^{3+} \rightarrow Mn^{2+}$. The $NaYF_4$:Nd(20 mol%) shell layer also supports $Mn^{2+}$ upconversion emission under excitation at 980 nm (Supplementary Fig. 18b). Notably, the core-shell-shell nanoparticles of its cubic equivalent could not generate $Mn^{2+}$ upconversion emission under laser irradiation at 808 nm (Supplementary Fig. 19).

To shed more light on creating short-lived color codes for $Mn^{2+}$-doped nanoparticles under both 808 and 980 nm excitations, we investigated $NaGdF_4$:Mn(30 mol%)@$NaGdF_4$:Yb/Tm(49/1 mol%)@$NaYF_4$:Nd(20 mol%) nanoparticles involving energy relay through $Nd^{3+} \rightarrow Yb^{3+} \rightarrow Er^{3+}$ (Fig. 3e). We found that the epitaxial growth of $NaYF_4$:Nd/Yb/Er with different dopant ratios onto $NaGdF_4$:Mn@$NaGdF_4$:Yb/Tm@$NaYF_4$:Nd nanoparticles can lead to a marked change in color output, while

retaining long-lived emission nature of $Mn^{2+}$ (Fig. 3f and Supplementary Fig. 20). Note that the excitation of both $Tm^{3+}$ and $Mn^{2+}$ ions at 808 nm can be largely suppressed by introducing an inert layer of $NaYF_4$ between $NaGdF_4$:Yb/Tm (49/1 mol%) and $NaYF_4$:Nd(20 mol%). This rendered the as-prepared multilayer nanoparticles with a white color output on 980 nm excitation, but a dominant yellow emission on 808 nm excitation (Supplementary Fig. 21).

**Multilevel anti-counterfeiting application**. The ability of our multilayer nanoparticles to simultaneously exhibit short- and long-lived emissions under excitation at either 980 or 808 nm offers a new class of optical materials ideal for multilevel authentication against product counterfeiting. As a proof-of-concept experiment, we made two-dimensional (2D) covert patterns on a reproduced artwork by stamping $Mn^{2+}$-doped core-shell nanoparticles of different composition (Fig. 4a). As a control, colloidal $NaYF_4$:Yb/Er(20/2 mol%) nanoparticles were also synthesized for the preparation of conventional upconversion anti-counterfeiting ink (Supplementary Fig. 22).

We found that a steady irradiation with a 980 nm laser (6 W $cm^{-2}$) leads to multicolor patterns displaying characteristic emissions of lanthanide and $Mn^{2+}$ emitting ions (Fig. 4a). Interestingly, dynamic scanning of the same patterns with a focused laser beam (at 64 W $cm^{-2}$) yielded different emission patterns (Fig. 4b). For instance, only a main green spot of emission emerged from pattern i made with $NaYF_4$:Yb/Er(20/2 mol%) nanoparticles, while an additional tailed emission in green was observed from other patterns (ii to vi, Supplementary Movie 1). More importantly, the color output of the main spot emission can be varied from red (pattern ii) to white (pattern vi) by controlling the doping composition of the lanthanides. As an added benefit, steady irradiation or dynamic scanning at 808 nm of the patterns iv and v made with $Nd^{3+}$-sensitized nanoparticles resulted in emission features that are comparable to those obtained on 980 nm excitation.

It is important to note that the binary color codes with a tailed emission are difficult to obtain by excitation of a pattern comprising a simple mixture of $NaYF_4$:Yb/Tm (20/0.2 mol%) nanoparticles and $SrAl_2O_4$:$Eu^{2+}$/$Dy^{3+}$ afterglow material. Although a blue upconversion emission can be observed from the pattern upon 980 nm excitation, dynamic laser scanning of the same area only offered a main spot of $Tm^{3+}$ emission (Supplementary Fig. 23a, b). This observation suggests a weak energy transfer from the upconversion nanoparticles to the afterglow materials under investigation. This hypothesis is confirmed by the result that ultraviolet irradiation is more effective in generating a yellow-green afterglow signal relative to indirect excitation with a 980 nm laser (Supplementary Fig. 23c, d). Taken together, these results confirm that as-prepared $Mn^{2+}$-doped upconversion nanoparticles are particularly promising for multilevel anti-counterfeiting applications without the need for time-gated set-up to separate and decode security data.

## Discussion

Our findings provide a new design for the creation of binary upconversion colors with two distinct timescales, which can be harnessed for data storage and security applications. This capability is enabled by combining a long-lived $Mn^{2+}$ luminescence and short-lived lanthanide emission at the single particle level through core-shell engineering. Considering the advantages associated with 808 nm excitation for deep tissue penetration and with a concomitant long-lived luminescence, the advent of these $Mn^{2+}$-doped nanoparticles may also have important implications for better in vivo cell tracking. Lastly, our synthetic strategy may offer a new, general route to prepare upconversion nanocrystals containing transition metal ions.

## Methods

**Preparation of $Mn^{2+}$-doped multilayer nanocrystals**. The $Mn^{2+}$-doped hexagonal-phased $NaGdF_4$ core nanoparticles were prepared through a hydrothermal method. Epitaxial growth of $NaGdF_4$:Yb/Tm(49/1 mol%) and $NaYF_4$ or $NaYF_4$: Nd (Eu, Eu/Tb or Tb) onto the as-prepared core nanoparticles was enabled by a combination of the coprecipitation and thermal decomposition methods. Detailed experimental procedure for the preparation of different types of $Mn^{2+}$-doped nanoparticles is provided in the Supplementary Methods.

**Preparation of ink solutions**. The as-prepared nanoparticles were treated with in a mixed solution of ethanol (0.5 mL) and HCl (0.5 mL, 2 M) to remove surface ligands[53]. The ligand-free nanoparticles were collected by centrifugation at 16,500 rpm for 20 min, and were dispersed into a mixed solution of water (0.1 mL) and dimethyl sulfoxide (0.1 mL). For preparation of security ink solution containing both lanthanide-doped upconversion nanoparticles and afterglow luminescent materials, the as-prepared dispersion of $NaYF_4$:Yb/Tm nanoparticles was added into a plastic tube (2.0 mL) charged with $SrAl_2O_4$:$Eu^{2+}$/$Dy^{3+}$ (10 mg). The mixture was sonicated for 15 min prior to use.

**Instrumentation**. TEM measurement was carried out on a field emission transmission electron microscope (JEOL-JEM 2010F) operated at an acceleration voltage of 200 kV. Powder X-ray diffraction patterns were recorded on a Bruker D8 Advance diffractometer using graphite-monochromatized CuKα radiation ($\lambda = 1.5406$ Å). Luminescence spectra were measured with a DM150i monochromator equipped with a R928 photon-counting photomultiplier tube, in conjunction with a 980-nm diode laser. The decay curves were measured with a customized phosphorescence lifetime spectrometer (FSP920-C, Edinburgh), equipped with a digital oscilloscope (TDS3052B, Tektronix) and a tunable mid-band OPO laser as an excitation source (410–2400 nm, Vibrant 355II, OPOTEK).

**Data availability**. The authors declare that the data that support the findings of this study are available within the article and its Supplementary Information files. All other relevant data are available from the corresponding author upon request.

Received: 14 February 2017 Accepted: 4 August 2017
Published online: 12 October 2017

## References

1. Höppe, H. A. Recent developments in the field of inorganic phosphors. *Angew. Chem. Int. Ed.* **48**, 3572–3582 (2009).
2. Bünzli, J. C. G. & Piguet, C. Taking advantage of luminescent lanthanide ions. *Chem. Soc. Rev.* **34**, 1048–1077 (2005).
3. Gai, S., Li, C., Yang, P. & Lin, J. Recent progress in rare earth micro/nanocrystals: soft chemical synthesis, luminescent properties, and biomedical applications. *Chem. Rev.* **114**, 2343–2389 (2014).
4. Chen, G., Qiu, H., Prasad, P. N. & Chen, X. Upconversion nanoparticles: design, nanochemistry, and applications in theranostics. *Chem. Rev.* **114**, 5161–5214 (2014).
5. Zhou, L. et al. Single-band upconversion nanoprobes for multiplexed simultaneous in situ molecular mapping of cancer biomarkers. *Nat. Commun.* **6**, 6938 (2015).
6. Gorris, H. H. & Wolfbeis, O. S. Photon-upconverting nanoparticles for optical encoding and multiplexing of cells, biomolecules, and microspheres. *Angew. Chem. Int. Ed.* **52**, 3584–3600 (2013).
7. Wang, J. et al. Photon energy upconversion through thermal radiation with the power efficiency reaching 16%. *Nat. Commun.* **5**, 5669 (2014).
8. Manor, A., Kruger, N., Sabapathy, T. & Rotschild, C. Thermally enhanced photoluminescence for heat harvesting in photovoltaics. *Nat. Commun.* **7**, 13167 (2016).
9. Liu, J. et al. Ultrasensitive nanosensors based on upconversion nanoparticles for selective hypoxia imaging in vivo upon near-infrared excitation. *J. Am. Chem. Soc.* **136**, 9701–9709 (2014).
10. Lee, J. et al. Universal process-inert encoding architecture for polymer microparticles. *Nat. Mater.* **13**, 524–529 (2014).
11. Wang, F. et al. Simultaneous phase and size control of upconversion nanocrystals through lanthanide doping. *Nature* **463**, 1061–1065 (2010).
12. Zhu, X. et al. Temperature-feedback upconversion nanocomposite for accurate photothermal therapy at facile temperature. *Nat. Commun.* **7**, 10437 (2016).
13. Dong, H. et al. Lanthanide nanoparticles: from design toward bioimaging and therapy. *Chem. Rev.* **115**, 10725–10815 (2015).

14. Fischer, S., Bronstein, N. D., Swabeck, J. K., Chan, E. M. & Alivisatos, A. P. Precise tuning of surface quenching for luminescence enhancement in core-shell lanthanide-doped nanocrystals. *Nano Lett.* **11**, 7241–7247 (2016).
15. Deng, R. et al. Temporal full-colour tuning through non-steady-state upconversion. *Nat. Nanotechnol.* **10**, 237–242 (2015).
16. Qin, X., Liu, X., Huang, W., Bettinelli, M. & Liu, X. Lanthanide-activated phosphors based on 4f-5d optical transitions: theoretical and experimental aspects. *Chem. Rev.* **117**, 4488–4527 (2017).
17. Liu, Y., Wang, D., Shi, J., Peng, Q. & Li, Y. Magnetic tuning of upconversion luminescence in lanthanide-doped bifunctional nanocrystals. *Angew. Chem. Int. Ed.* **52**, 4366–4369 (2013).
18. Zhao, J. B. et al. Single-nanocrystal sensitivity achieved by enhanced upconversion luminescence. *Nat. Nanotechnol.* **8**, 729–734 (2013).
19. Zheng, W. et al. Lanthanide-doped upconversion nano-bioprobes: electronic structures, optical properties, and biodetection. *Chem. Soc. Rev.* **44**, 1379–1415 (2015).
20. Haase, M. & Schäfer, H. Upconverting nanoparticles. *Angew. Chem. Int. Ed.* **50**, 5808–5829 (2011).
21. Zhou, B., Shi, B., Jin, D. & Liu, X. Controlling upconversion nanocrystals for emerging applications. *Nat. Nanotechnol.* **10**, 924–936 (2015).
22. Rodríguez-Sevilla, P. et al. Optical torques on upconverting particles for intracellular microrheometry. *Nano Lett.* **16**, 8005–8014 (2016).
23. Lu, Y. et al. Tunable lifetime multiplexing using luminescent nanocrystals. *Nat. Photon.* **8**, 32–36 (2014).
24. Lu, Y. et al. On-the-fly decoding luminescence lifetimes in the microsecond region for lanthanide-encoded suspension arrays. *Nat. Commun.* **5**, 3741 (2014).
25. Deng, R. & Liu, X. Optical multiplexing: tunable lifetime nanocrystals. *Nat. Photon.* **8**, 10–12 (2014).
26. Liu, F., Liang, Y. & Pan, Z. Detection of up-converted persistent luminescence in the near infrared emitted by the $Zn_3Ga_2GeO_8$: $Cr^{3+}$, $Yb^{3+}$, $Er^{3+}$ phosphor. *Phys. Rev. Lett.* **113**, 177401 (2014).
27. Zeng, S. et al. Simultaneous realization of phase/size manipulation, upconversion luminescence enhancement, and blood vessel imaging in multifunctional nanoprobes through transition metal $Mn^{2+}$ doping. *Adv. Funct. Mater.* **24**, 4051–4059 (2014).
28. Wang, J., Wang, F., Wang, C., Liu, Z. & Liu, X. G. Single-band upconversion emission in lanthanide-doped $KMnF_3$ nanocrystals. *Angew. Chem. Int. Ed.* **50**, 10369–10372 (2011).
29. Tian, G. et al. $Mn^{2+}$ dopant-controlled synthesis of $NaYF_4$:Yb/Er upconversion nanoparticles for in vivo imaging and drug delivery. *Adv. Mater.* **24**, 1226–1231 (2012).
30. Maldiney, T. et al. Controlling electron trap depth to enhance optical properties of persistent luminescence nanoparticles for in vivo imaging. *J. Am. Chem. Soc.* **133**, 11810–11815 (2011).
31. Vink, A. P., Bruin, M. Ad, Roke, S., Peijzel, P. S. & Meijerink, A. Luminescence of exchange coupled pairs of transition metal ions. *J. Electrochem. Soc.* **148**, E313–E320 (2001).
32. Li, Y., Gecevicius, M. & Qiu, J. Long persistent phosphors-from fundamentals to applications. *Chem. Soc. Rev.* **45**, 2090–2136 (2016).
33. Zhang, C. & Lin, J. Defect-related luminescent materials: synthesis, emission properties and applications. *Chem. Soc. Rev.* **41**, 7938–7961 (2012).
34. Ma, H. et al. High-quality sodium rare-earth fluoride nanocrystals: controlled synthesis and optical properties. *J. Am. Chem. Soc.* **128**, 6426–6436 (2006).
35. Nam, S. H. et al. Long-term real-time tracking of lanthanide ion doped upconverting nanoparticles in living cells. *Angew. Chem. Int. Ed.* **50**, 6093–6097 (2011).
36. Han, S. et al. Multicolour synthesis in lanthanide-doped nanocrystals through cation exchange in water. *Nat. Commun.* **7**, 13059 (2016).
37. Liu, D. et al. Three-dimensional controlled growth of monodisperse sub-50 nm heterogeneous nanocrystals. *Nat. Commun.* **7**, 10254 (2016).
38. Johnson, N. J. J., Korinek, A., Dong, C. & van Veggel, F. C. J. M. Self-focusing by ostwald ripening: a strategy for layer-by-layer epitaxial growth on upconverting nanocrystals. *J. Am. Chem. Soc.* **134**, 11068–11071 (2012).
39. Boyer, J. C., Vetrone, F., Cuccia, L. A. & Capobianco, J. A. Synthesis of colloidal upconverting $NaYF_4$ nanocrystals doped with $Er^{3+}$, $Yb^{3+}$ and $Tm^{3+}$, $Yb^{3+}$ via thermal decomposition of lanthanide trifluoroacetate precursors. *J. Am. Chem. Soc.* **128**, 7444–7445 (2006).
40. Wang, F., Deng, R. & Liu, X. Preparation of core-shell $NaGdF_4$ nanoparticles doped with luminescent lanthanide ions to be used as upconversion-based probes. *Nat. Protoc.* **9**, 1634–1644 (2014).
41. Chan, E. M. Combinatorial approaches for developing upconverting nanomaterials: high-throughput screening, modeling, and applications. *Chem. Soc. Rev.* **44**, 1653–1679 (2015).
42. Huang, P. et al. Lanthanide-doped $LiLuF_4$ upconversion nanoprobes for the detection of disease biomarkers. *Angew. Chem. Int. Ed.* **53**, 1252–1257 (2014).
43. Wang, F. et al. Tuning upconversion through energy migration in core-shell nanoparticles. *Nat. Mater.* **10**, 968–973 (2011).
44. Li, X. et al. Energy migration upconversion in manganese(II)-doped nanoparticles. *Angew. Chem. Int. Ed.* **54**, 13312–13317 (2015).
45. Wen, H. et al. Upconverting near-infrared light through energy management in core-shell-shell nanoparticles. *Angew. Chem. Int. Ed.* **52**, 13419–13423 (2013).
46. Zhang, C. & Lee, J. Y. Prevalence of anisotropic shell growth in rare earth core-shell upconversion nanocrystals. *ACS Nano* **7**, 4393–4402 (2013).
47. Gao, G. & Wondraczek, L. Near-infrared down-conversion in $Mn^{2+}$–$Yb^{3+}$ co-doped $Zn_2GeO_4$. *J. Mater. Chem. C* **1**, 1952–1958 (2013).
48. Zhou, B. et al. Constructing interfacial energy transfer for photon up- and down-conversion from lanthanides in a core-shell nanostructure. *Angew. Chem. Int. Ed.* **55**, 12356–12360 (2016).
49. Zhang, Y. et al. Multicolor barcoding in a single upconversion crystal. *J. Am. Chem. Soc.* **136**, 4893–4896 (2014).
50. Wang, Y. et al. $Nd^{3+}$-sensitized upconversion nanophosphors: efficient *in vivo* bioimaging probes with minimized heating effect. *ACS Nano* **7**, 7200–7206 (2013).
51. Xie, X. et al. Mechanistic investigation of photon upconversion in $Nd^{3+}$-sensitized core-shell nanoparticles. *J. Am. Chem. Soc.* **135**, 12608–12611 (2013).
52. Shen, J. et al. Engineering the upconversion nanoparticle excitation wavelength: cascade sensitization of tri-doped upconversion colloidal nanoparticles at 800 nm. *Adv. Opt. Mater.* **1**, 644–650 (2013).
53. Bogdan, N., Vetrone, F., Ozin, G. A. & Capobianco, J. A. Synthesis of ligand-free colloidally stable water dispersible brightly luminescent lanthanide-doped upconverting nanoparticles. *Nano Lett.* **11**, 835–840 (2011).


## Acknowledgements

This work is supported by the Singapore Ministry of Education (Grant R143000627112, R143000642112), Agency for Science, Technology and Research (A*STAR) under the contracts of 122-PSE-0014 and 1231AFG028 (Singapore), National Research Foundation, Prime Minister's Office, Singapore under its Competitive Research Program (CRP Award No. NRF-CRP15-2015-03), National Basic Research Program of China (973 Program, Grant 2015CB932200), National Natural Science Foundation of China (21471109 and 21210001), Natural Science Foundation of Jiangsu Province (BE2015699), and the CAS/SAFEA International Partnership Program for Creative Research Teams.

## Author contributions

X.W.L. conceived the project. L.H., A.H.A., H.Z., and X.G.L. supervised the project. X.W. L., X.J.X., D.T.B.L., S.Y.S., and D.Y.F. designed the experiments. X.G.L. and L.L.L. carried out the spectral measurement experiment. X.W.L., Z.G.Y., and X.Y.L. performed the nanocrystal synthesis. R.D. carried out simulation work. X.W.L. and Y.W. conducted the anti-counterfeiting applications. X.W.L. and X.G.L. wrote the manuscript with input from other authors.

## Additional information

**Supplementary Information** accompanies this paper at doi:10.1038/s41467-017-00916-7.

**Competing interests:** The authors declare no competing financial interests.